*Advances in Engineering Research, volume 209*
**International Joint Conference on Science and Engineering 2021 (IJCSE 2021)**

# Identification of the Activated Fault Plane of the 16 June 2021 Earthquake (Mw=5.9) in the Banda Sea

Muhammad N. Fahmi[1] Madlazim[1,*] Dyah P. Sari[2]

[1]*Departement of Physics, Universitas Negeri Surabaya, Indonesia*
[2]*Departement of Science Education, Universitas Negeri Surabaya, Indonesia*
[*]*Corresponding author. Email: madlazim@unesa.ac.id*

**ABSTRACT**
On 16 June 2021, a moderate earthquake with Mw 5.9 occurred in the Banda Sea, precisely at the top of the Banda Arc. The fault plane mechanism in this area is still not well identified, and this problem can be solved by determining the activated fault plane. In this research, the activated fault plane was based on the estimation of rupture directivity of the earthquake using the curve fitting method between observed and calculated P-wave rupture duration data. The maximum epicentral distance between the station and the epicentre of the earthquake is 40°. The number of seismic stations used is 33 stations with good azimuthal coverage. The rupture directivity of the earthquake is towards the south-southwest (SSW) with an azimuth of 196.5° ± 3.3°. This research has activated fault plane results validated using five aftershocks epicentres from USGS and NP1 CMT catalogue from GEOFON. The consistent NP is NP1 with strike/dip/slip values, respectively as follows 217/57/-85. This research also revealed that the earthquake located at the top of the Band Arc had an SSW-NNE fault orientation.

***Keywords:*** *Rupture directivity, Activated fault plane, Banda Arc, Rupture duration, P-wave.*

## 1. INTRODUCTION

The earthquake's size is theoretically proportional to the area of the fault where the effective slip occurs. Medium earthquakes (Mw > 5) usually have a fault length of several tens of kilometres, while for large earthquakes (Mw > 7), the fault length is several tens to hundreds of kilometres. An important thing that is rarely considered in determining the source mechanism for moderate earthquakes because they have a less significant impact than large earthquakes. However, it is essential to know because moderate earthquakes occur more globally than large earthquakes. One of them was the earthquake on 16 June 2021, which occurred in the Banda Sea at 7.0 km. This earthquake has a typical fault type occurring in one of the most striking subduction zones globally, with a concave-westward arc bending 180° within a tight 300 km radius of curvature (Figure 1). The history of seismicity in the Banda Sea in the past can cause large earthquakes and tsunamis that can destroy the Banda Islands [1, 2], as well as potential threats that will occur in the future [3, 4, 5], should be associated with megathrusts along the outer Banda Arc. However, because the Banda Arc is an arc-continental collision zone, it no longer has oceanic trenches and thus does not have megathrusts [6, 7, 8, 9]. Therefore, the source mechanism of the earthquake on 16 June 2021 is crucial because it can be used as further knowledge regarding geological conditions in the Banda Sea.

Determination of the activated fault plane is critical because it can be used as further knowledge regarding the mechanism of earthquake sources [10,11]. The Centroid Moment Tensor (CMT) solution produces two fault planes: the activated fault plane and the auxiliary fault plane, which are equivalent and indistinguishable. Identification of the activated fault plane of the CMT solution can lead to fault plane ambiguity. In order to select one of the two nodal planes (NP), we need additional information such as aftershock distribution or rupture dimension mapping at ground level. When none of this information is available, it is usually forced to make predictions based on local geological (or tectonic) conditions. Nevertheless, this has many drawbacks and has enormous potential for causing errors in determining the activated fault plane. The solution to overcome this is to determine the rupture directivity of the earthquake [12] because the rupture propagates along the fault plane [13].

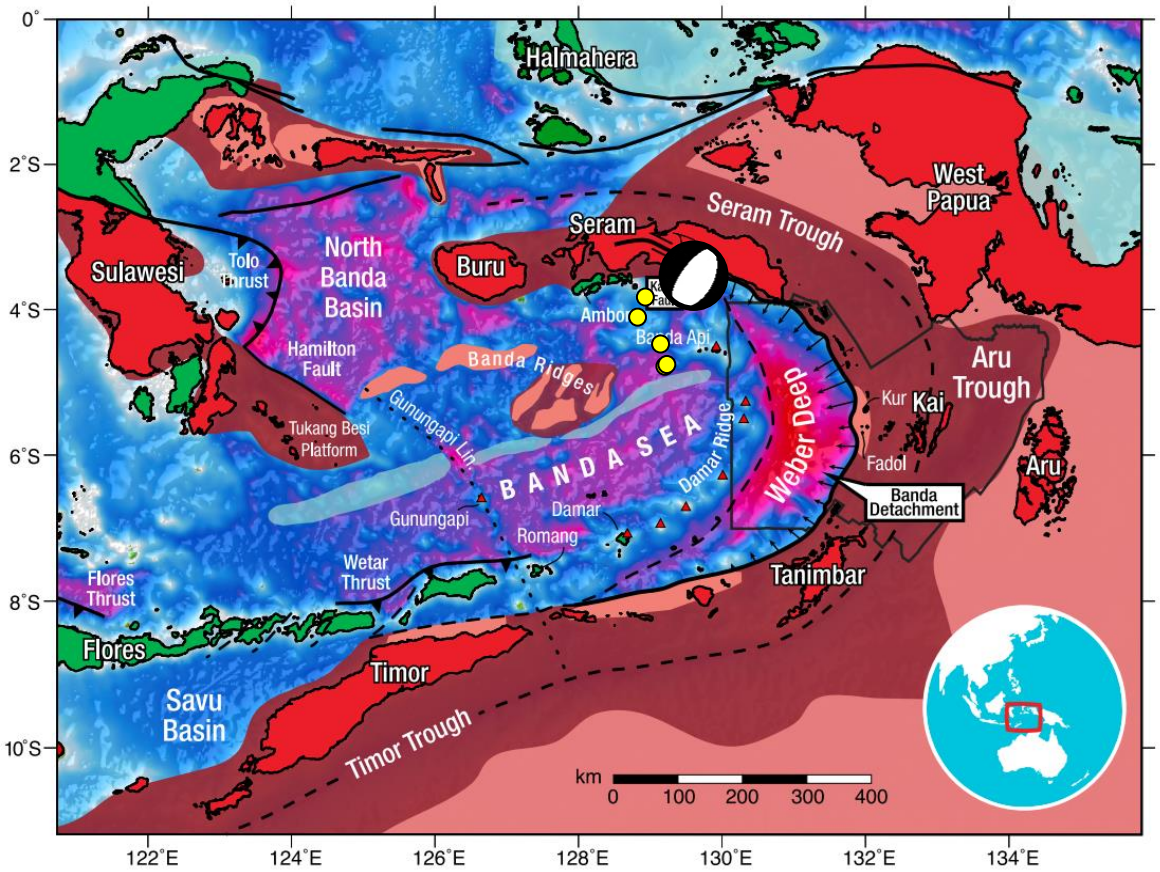


**Figure 1** The current geological map of the Banda Sea, modified from Pownall et al. (2016) [14]. Beachball represents the 16 June 2021 earthquake, and the yellow circle is the distribution of aftershocks.

The earthquake of 16 June 2021 is moderate. Usually, determining the rupture directivity for a moderate earthquake is using differences in source duration [15,16] or peak ground amplitude [17,18] observed at each station in the time domain or the difference in spectral ratios [19,20], or it could be used corner frequencies in the frequency domain [21]. These parameters contain information about the earthquake fault characteristics. Therefore, it is possible to determine the activated fault plane and to estimate the rupture directivity by analyzing data from each station with good azimuthal coverage.

This research aims to determine the activated fault plane of the 16 June 2021 earthquake in the Banda Sea through a rupture approach. Estimation of earthquake rupture directivity using curve fitting method between observed and calculated P-wave rupture duration. Furthermore, the results of the rupture directivity in this research will be validated using data on the distribution of aftershocks and local geological conditions.

## 2. METHODS

The data used in this research is secondary data obtained from the https://ds.iris.edu/wilber3/find_event page. The maximum epicentral distance between the earthquake epicentre and the station is 40°. The rupture duration was recorded by 33 stations which were spread evenly around the earthquake epicentre. The rupture directivity can be determined by the curve fitting between observed and calculated rupture durations. In particular, the rupture directivity is characterized by the minimum rupture duration recorded at the station. Mathematically, the rupture duration can be determined using Equation 1.

$$T_{dur} = \frac{L}{V_r} - \frac{L}{V_p} cos\ cos\ (\varphi - \lambda^*) \quad (1)$$

where $L$ is the rupture length, $V_r$ denotes the rupture velocity, $V_p$ indicates the P-wave velocity, $\varphi$ describes the station azimuth angle, and $\lambda^*$ represents the rupture directivity angle. If the value of the difference between $\varphi$ and $\lambda^*$ is equal to zero or minimum, then the resulting cosine value will be maximum. Thus, the minimum rupture duration can be obtained.

P-wave is a seismic wave that has the highest velocity of other seismic waves. Thus, it can be used as an estimation of the rupture directivity quickly and accurately. In this study, the P-wave is used to estimate

the rupture duration with a direct procedure, namely by calculating the delay time after the arrival of the P-wave by 90% ($T^{0.9}$), 80% ($T^{0.8}$), 50% ($T^{0.5}$), dan 20% ($T^{0.2}$) from the peak value [22,23]. The rupture duration of P-wave can be estimated using the following equation:

$$T_{dur} = (1 - w)T^{0.9} + w\,T^{0.2} \quad (2)$$

$$w = \frac{\left[\frac{T^{80} + T^{50}}{2} - 20\,s\right]}{40s} \quad (3)$$

where $w$ is a constant, which is mathematically represented in Equation (3) with a limit $0 \leq w \leq 1$. Furthermore, the rupture duration value limit is $T^{0.2} \leq T_{dur} \leq T^{0.9}$ [24].

## 3. RESULTS AND DISCUSSION

The estimated rupture directivity for the 16 June 2021 earthquake uses teleseismic data, with a maximum epicentral distance of 40°. Teleseismic data is used because it can reach station coverage that can cover the epicentre well. The closer the distance between stations, the rupture directivity results more accurate. The estimation results of the rupture duration of the P-wave were processed using non-linear inversion to obtain the curve fitting results also the model parameters of the rupture directivity. The curve fitting results of the 16 June 2021 earthquake are presented in Figure 2.

According to Eq. 1, the rupture directivity can be estimated from the minimum rupture duration recorded at the station [25]. The minimum rupture duration in this earthquake is 0.95 s which is located at an azimuth of 199.95°. Figure 2 describes that the observed rupture duration data (grey circle) and calculated rupture duration data (black line) have a good match. This is indicated by the R-squared value of 0.979. In addition, it is supported by the RMSE value of 4.684. This figure also represents that the shape of the curve from the calculation data represent the cosine curve, which is characteristic of the unilateral rupture duration equation. This result has similar to the research of Caldeira et al. (2010) [26] and López-Comino et al. (2016) [27] by using different fitting methods. Based on the curve fitting results, it can be seen that the minimum peak of the curve is located at ~200° azimuth. This is correlated with the resulting rupture directivity model parameter, located at 196.5° ± 3.3° azimuth. The uncertainty of the model parameters is relatively small, so it can be indicated that the resulting model parameters are accurate. When we compare, the result of the rupture directivity using rupture duration and those using curve fittings have the same results. Thus, on 16 June 2021, the earthquake ruptured directivity is towards the south-southwest (SSW) at an azimuth of around 196.5° ± 3.3°.

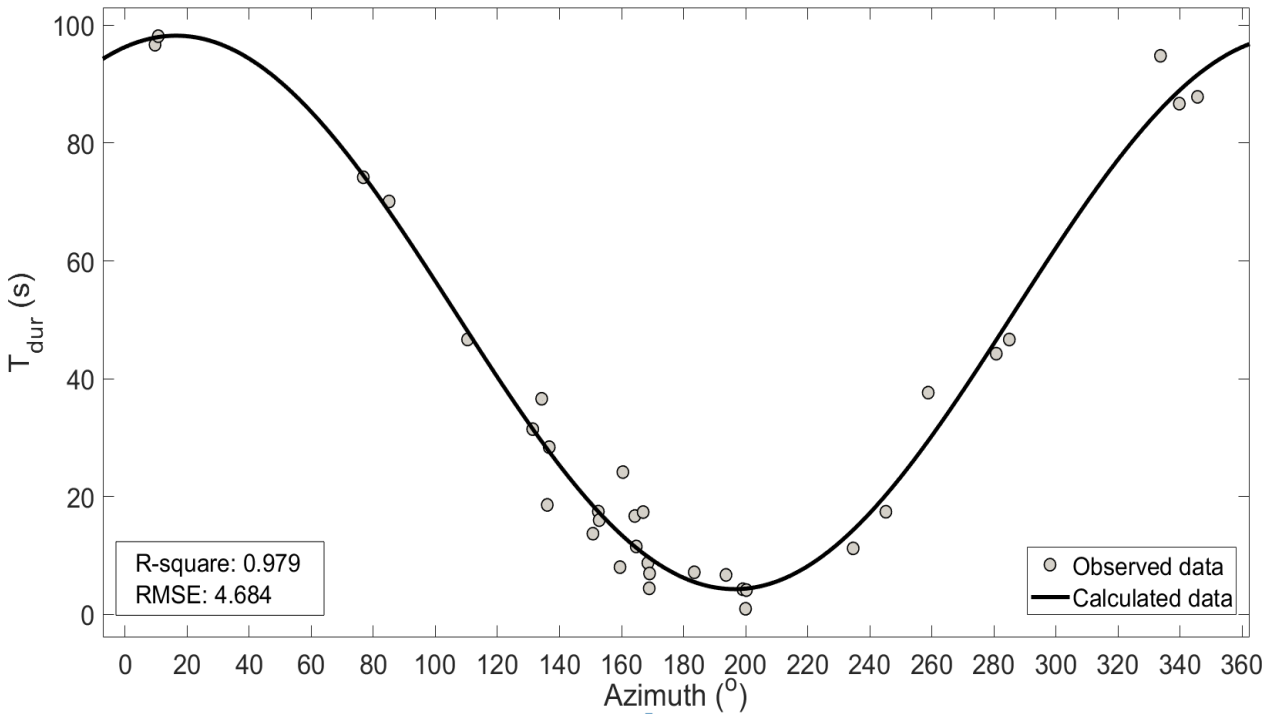


**Figure 2** The curve fitting results between observed and calculated rupture duration of the 16 June 2021 earthquake.

The rupture directivity can determine the activated fault plane, whether the earthquake has a reverse, normal, and strike-slip focal mechanism. In this case, the 16 June 2021 earthquake has a typical fault type. The activated fault plane is determined by comparing the two focal mechanism strike angles with the rupture directivity angle. The striking angle with the exact match or closes to the rupture directivity can indicate an activated fault plane. A comparison of focal mechanism strike with rupture directivity has presented in Table 1.

**Table 1.** Comparison of focal mechanism strike angle with rupture directivity

| Source | Nodal Plane 1[a] | | | Nodal Plane 2[a] | | | Rupture Directivity |
|---|---|---|---|---|---|---|---|
| | S | D | R | S | D | R | |
| GCMT[b] | 246 | 45 | -48 | 14 | 58 | -124 | 196,5° ± 3,3° |
| USGS[c] | 217 | 57 | -85 | 27 | 34 | -98 | |
| GFZ[d] | 227 | 37 | -79 | 34 | 52 | -98 | |

[a]S (Strike), D (Dip), and R (Rake)
[b]GCMT : https://www.globalcmt.org/
[c]USGS : https://earthquake.usgs.gov/earthquakes/search/

Table 1 describes that the three international seismological institutions (GCMT, USGS, GFZ) have the same focal mechanism values for the 16 June 2021 earthquake. Based on the focal mechanism solution, it can be seen that the angle of rupture directivity is closer to the strike value of NP 1 than NP 2. The closeness of rupture directivity angle to the NP strike value indicates that this earthquake has an activated plane located on the nodal plane 1, which has a strike value is 217° (USGS solution). If we noted the dip value of NP1 from the three earthquakes CMT catalogues, none of them has a dip value above 60°, some even 37°. These have a good agreement with the characteristic of Low Angle Normal Fault (LANF) in the Banda Sea [28]. The results of rupture directivity and the activated fault plane are also supported by the distribution of aftershocks (Figure 1 yellow circle) located in the south-southwest (SSW) direction from the epicentre. It confirms that the fault plane of this earthquake has an SSW-NNE fault orientation. Several previous studies have also revealed that the propagation area of the rupture directivity and the activated fault plane are areas where aftershocks occur [29, 30, 11].

Based on the geological conditions, this earthquake is located at the top of the Banda Arc. In this area, the fault plane mechanism has not yet been identified. According to Axen (1999) [31] and Webber et al. (2020) [32], there is a possibility that an earthquake at the top of Banda Arc has the potential to have a normal fault type which has a steeper dip value (>30°). The results of this study proved this possibility, where the earthquake that occurred above the Banda Arc had a strike orientation of ~200° and had a dip value of >30°. Thus, the results of the estimation of the activated fault plane using the rupture directivity are reliable.

## 4. CONCLUSION

The rupture directivity of the earthquake can estimate the activated fault plane of the 16 June 2021 earthquake. Based on the results of non-linear inversion of rupture duration by the curve fitting method, the rupture directivity propagates in the south-southwest (SSW) direction at an azimuth of 196.5° ± 3.3°. The angle of rupture directivity obtained indicates the actual fault plane, located at NP 1, with a strike/dip/rake value are 217/57/-85, respectively. This research can also prove that the earthquake at the top of Band Arc has an SSW-NNE fault orientation. Determination of rupture directivity depends on the density of station that records seismic waves. The closer the positions of stations around the epicentre, the more accurate the rupture directivity results. For future research, the rupture directivity can be developed to predict aftershocks in real-time and hazard mitigation.

## AUTHORS' CONTRIBUTIONS

Muhammad Nurul Fahmi: conceptualization, method, drafting manuscript, data visualization; Madlazim: Review and editing of manuscript; and Dyah Permata Sari: data curation, and editing.

## ACKNOWLEDGMENTS

The authors sincerely thank the United States Geological Survey (USGS) for providing data on the focal mechanism of earthquakes and aftershocks, the German Research Center for Geosciences (GFZ) and The Global Centroid-Moment-Tensor (GCMT) for providing data on earthquake focal mechanisms.

## REFERENCES

[1] T.L. Fisher, R.A. Harris, Reconstruction of 1852 Banda Arc Megathrust Earthquake and Tsunami,

Natural Hazard, 83 (2016) 667—689. DOI: https://doi.org/10.1007/s11069-016-2345-6

[2] Z. Y-C. Liu, R.A. Harris, Discovery of Possible Mega-thrust Earthquake Along the Seram Trough from Records of 1629 Tsunami in Eastern Indonesian Region, 72 (2014) 1311—1328. DOI: https://doi.org/10.1007/s11069-013-0597-y

[3] F. Løvholt, D. Kühn, H. Bungum, C.B. Harbitz, S. Glimsdal, Historical tsunamis and present tsunami hazard in eastern Indonesia and the southern Philippines, Journal of Geophysical Research Solid Earth, 117(B9) (2012). DOI: https://doi.org/10.1029/2012JB009425

[4] F. Løvholt, N.J. Setiadi, J. Birkmann, C.B. Harbitz, C. Bach, N. Fernando, G. Kaiser, F. Nadim, Tsunami risk reduction - are we better prepared today than in 2004?, International Journal Disaster Risk Reduction, 10 (2014) 127-142. DOI: 10.1016/j.ijdrr.2014.07.008

[5] N. Horspool, I. Pranantyo, J. Griffin, H. Latief, D.H. Natawidjaja, W. Kongko, A. Cipta, B. Bustaman, S.D. Anugrah, H.K. Thio, A Probalistic Tsunami Hazard Assessment for Indonesia, Natural Hazards and Earth System Sciences, 14(11) (2014) 3105–3122. DOI: https://doi.org/10.5194/nhess-14-3105-2014

[6] D.J. Carter, M.G. Audley-Charles, A.J. Barber, Stratigraphical Analysis of Island Arc—Continental Margin Collision in Eastern Indonesia, Journal of the Geological Society, 132(2) (1976) 179—198. DOI: https://doi.org/10.1144/gsjgs.132.2.0179

[7] A.N. Richardson, D.J. Blundell, A.N. Richardson, Continental Collision in the Banda Arc, in R. Hall, D.J. Bundell (Eds), Geological Society London Special Publications, 106 (1996), 47—60. DOI: http://dx.doi.org/10.1144/GSL.SP.1996.106.01.05

[8] M.G. Audley-Charles, Ocean Trench Blocked and Obliterated by Banda Forearc Collision with Australian Proximal Continental Slope, Tectonophysics, 389(1—2) 65—79. DOI: https://doi.org/10.1016/j.tecto.2004.07.048

[9] W. Spakman, R. Hall, Surface Deformation and Slab-mantle Interaction During Banda Arc Subduction Rollback, Nature Geoscience, 3 (2010) 562—566. DOI: https://doi.org/10.1038/ngeo917

[10] L.M. Warren, P.M. Shearer, Systematic Determination of Earthquake Rupture Directivity and Fault Planes from Analysis of Long-period P-wave Spectra, Geophysical Journal International, 164(1) 2006 46—62. DOI: https://doi.org/10.1111/j.1365-246X.2005.02769.x

[11] Madlazim, T. Prastowo T, M.N. Fahmi, Estimation of Rupture Directivity, CMT and Earthquake Tsunami Parameters and Their Correlation with the Main Source of the First Tsunami Wave, September 28, 2018. Science of Tsunami Hazards, 39(4) 2020 228—242. Retrieved from: www.tsunamisociety.org/STHVol39N4Y2020.pdf

[12] H. Kao, S-J. Shan, Rapid Identification of Earthquake Rupture Plane Using Source-scanning Algorithm, Geophysical Journal International, 168(3) (2007) 1011—1020. DOI: https://doi.org/10.1111/j.1365-246X.2006.03271.x

[13] N.A. Haskell, Total Energy and Energy Spectral Density of Elastic Wave Radiation from Propagating Faults, Bulletin of the Seismological Society of America, 54(6A) (1964) 1811—1841. DOI: https://doi.org/10.1785/BSSA05406A1811

[14] J.M. Pownall, R. Hall, G.S. Lister, Rolling Open Earth's Deepest Forearc Basin, Geology, 44(11) (2016) 947—950. DOI: https://doi.org/10.1130/G38051.1

[15] A.A. Velasco, C.J. Ammon, T. Lay, Empirical Green Function Deconvolution of Broadband Surface Waves: Rupture Directivity of the 1992 Landers, California (Mw=7.3), Earthquake, Bulletin of the Seismological Society of America, 84(3) (1994) 735—750. DOI: https://doi.org/10.1785/BSSA0840030735

[16] Y. Tan, D. Helmberger, Rupture Directivity Characteristica of the 2003 Big Bear Sequence, Bulletin of the Seismological Society of America, 100(3) (2010) 1089—1106. DOI: https://doi.org/10.1785/0120090074

[17] V. Convertito, M. Caccavale, R.D. Matteis, A. Emolo, D. Wald, A. Zollo, Fault Extent Estimation for Near-Real-Time Ground-Shaking Map Computation Purposes, Bulletin of the Seismological Society of America, 102(2) (2012) 661—679. DOI: https://doi.org/10.1785/0120100306

[18] I. Kurzon, F.L. Vernon, Y. Ben-Zion, G. Atkinson, Ground Motion Prediction Equations in the San Jacinto Fault Zone: Significant Effects of Rupture Directivity and Fault Zone Amplification, Pire and Applied Geophysics, 171 (2014) 3045—3081. DOI: https://doi.org/10.1007/s00024-014-0855-2

[19] E. Wang, A.M. Rubin, Rupture Directivity of Microearthquakes on the San Andreas Fault from Spectral Ratio Inversion, Geophysical Journal International, 186(2) (2011) 852—866. DOI: https://doi.org/10.1111/j.1365-246X.2011.05087.x

[20] Z.E. Ross, Y. Ben-Zion, Toward Reliable Automated Estimated of Earthquake Source Properties from Body Wave Spectra, Journal of Geophysical Research: Solid Earth, 121(6) 4390—4407. DOI: https://doi.org/10.1002/2016JB013003

[21] D.L. Kane, P.M. Shearer, B.P. Goertz-Allman, F.L. Vernon, Rupture Directivity of Small Earthquakes at Parkfield, Journal of Geophysical Research: Solid Earth, 118(1) 212-221. DOI: https://doi.org/10.1029/2012JB009675

[22] A. Lomax, A. Michelini, Tsunami Early Warning Using Earthquake Rupture Duration and P-wave Dominant Period: The Importance of Length and Depth of Faulting, Geophysical Journal International, 185(1) (2011) 283-291. DOI: https://doi.org/10.1111/j.1365-246X.2010.04916.x

[23] Madlazim, Toward Indonesian Tsunami Early Warning System by Using Rapid Rupture Durations Calculation, Science of Tsunami Hazards, 30(4) 233—243. Retrieved from: http://tsunamisociety.org/304Madlazim.pdf

[24] A. Lomax, A. Michelini, $M_{wpd}$: A Duration-amplitude Procedure for Rapid Determination of Earthquake Magnitude and Tsunamigenic Potential from P Waveforms, Geophysical Journal International, 176(1) (2009) 200—214. DOI: https://doi.org/10.1111/j.1365-246X.2008.03974.x

[25] R-D. Hwang, J-P Chang, C-Y Wang, J-J. Wu, C-H Kuo, Y-W. Tsai, W-Y. Chang, T-W. Lin, Rise Time and Source Duration of the 2008 $M_w$ 7.9 Wenchuan (China) Earthquake as Revealed by Rayleigh Waves, Earth Planets and Space, 63 (2011) 427—434. DOI: https://doi.org/10.5047/eps.2011.01.002

[26] B. Caldeira, M. Bezzeghoud, J.F. Borges, DIRDOP: A Directivity Approach to Determining the Seismic Rupture Velocity Vector, Journal of Seismology, 14 (2010) 565—600. DOI: https://doi.org/10.1007/s10950-009-9183-x

[27] J.A. López-Comino, D. Stich, J. Morales, A.M.G. Ferreira, Resolution of Rupture Directivity in Weak Events:1-D versus 2-D Source Parameterizations for the 2011, $M_w$ 4.6 and 5.2 Lorca Earthquakes Spain, Journal of Geophysical Research: Solid Earth, 121(9) (2016) 6608—6626. DOI: https://doi.org/10.1002/2016JB013227

[28] P.R. Cummins, I.R. Pranantyo, J.M. Pownall, J.D. Griffin, I. Meilano, S. Zhao, Earthquakes and Tsunamis Caused by Low-angle Normal Faulting in the Banda Sea Indonesia, Nature Geoscience, 13(2020) 312—318. DOI: https://doi.org/10.1038/s41561-020-0545-x

[29] Y. Yukutake, Y. Iio, Why Do Aftershocks Occur? Relationship Between Mainshock Rupture and Aftershock Sequence Based on Highly Resolved Hypocenter and Focal Mechanism Distributions, Earth Planets Space, 69 (2017) 1—15. DOI: https://doi.org/10.1186/s40623-017-0650-2

[30] W. Li, S. Ni, C. Zang, R. Chu, Rupture Directivity of the 2019 Mw 5.8 Changning Sichuan China Earthquake and Implication for Induced Seismicity, Bulletin of the Seismological Society of America, 110(5) (2020) 2138—2153. DOI: https://doi.org/10.1785/0120200013

[31] G.J. Axen, Low-angle Normal Fault Earthquakes and Triggering, Geophysical Research Letters, 26(24) (1999) 3693—3696. DOI: https://doi.org/10.1029/1999GL005405

[32] S. Webber, T.A. Little, K.P. Norton, J. Österle, M. Mizera, D. Sewad, G. Holden, Progressive Back-warping of a Rider Block Atop an Actively Axhuming Continental Low-angle Normal Fault, Journal of Structural Geology, 130 (2020). DOI: https://doi.org/10.1016/j.jsg.2019.103906